AUTHOR(S):

Kubo, Takuya; Shimonaka, Miwa; Watabe, Yoshiyuki; Akiyoshi, Kazunari; Balachandran, Jeyadevan; Otsuka, Koji

京都大学
KYOTO UNIVERSITY

京都大学学術情報リポジトリ
KURENAI 紅
Kyoto University Research Information Repository

Nanocomposites

Study on magnetic thermal seeds coated with thermal-responsive molecularly imprinted polymers

Takuya Kubo, Miwa Shimonaka, Yoshiyuki Watabe, Kazunari Akiyoshi, Jeyadevan Balachandran & Koji Otsuka

View supplementary material

Published online: 09 Dec 2021.

Submit your article to this journal

View related articles

View Crossmark data

京都大学
KYOTO UNIVERSITY

Taylor & Francis
Taylor & Francis Group

RESEARCH ARTICLE

OPEN ACCESS | Check for updates

Study on magnetic thermal seeds coated with thermal-responsive molecularly imprinted polymers

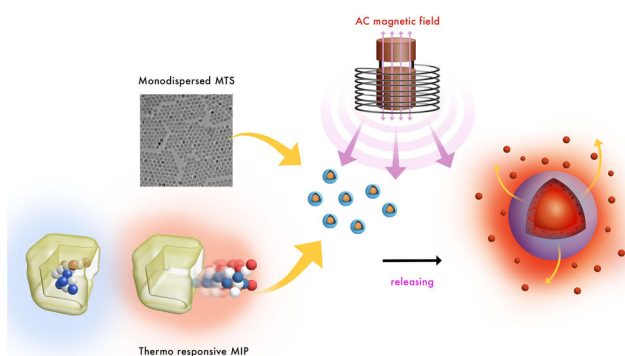Takuya Kubo[a] (iD), Miwa Shimonaka[a], Yoshiyuki Watabe[a,b], Kazunari Akiyoshi[c], Jeyadevan Balachandran[d] and Koji Otsuka[a] (iD)

[a]Department of Material Chemistry, Graduate School of Engineering, Kyoto University, Kyoto, Japan; [b]Research Center, Shimadzu General Service, Inc, Kyoto, Japan; [c]Department of Polymer Chemistry, Graduate School of Engineering, Kyoto University, Kyoto, Japan; [d]Department of Material Science, University of Shiga Prefecture, Hikone, Japan

ABSTRACT

We conceived a novel hybrid carrier of a thermal-responsive molecularly imprinted polymer (MIP) and a magnetic thermal seed (MTS) that showed a heat-generating ability under an alternate current (AC) magnetic field. Compared to our previous publications, we modify both the MIP and MTS to improve the feasibility for the hybrid carrier, briefly we have to achieve the accurate size control and narrower size distribution of MTS, and higher molecular recognition/release ability of MIP. Firstly, uniformly sized particles which are expected to show a large heat-generating ability under an AC magnetic field were successfully prepared by controlling the core creation. Then, an MIP targeted for selective adsorption of pemetrexed (PMX), a well-known anti-cancer drug, was prepared using N-carbobenzoxy-L-glutamic acid as a pseudo template. Finally, the preliminary hybridization of the MTS and the MIP-equivalent polymer coating was examined by introducing vinyl groups as methacrylic acid using a ligand exchanging method.

GRAPHICAL ABSTRACT

1. Introduction

Molecular imprinting technique, which enables creation of specific molecular recognition sites inside of a crosslinked polymer for selective adsorption of targeting compounds, has been widely studied in various fields [1–7]. The obtained polymer using this technique is called as a molecularly imprinted polymer (MIP), which is generally prepared by using the following procedures. (➜) Mixing the template molecules and functional monomers to form the complex by the interaction, (➜) Polymerization after adding the crosslinker to form a crosslinked polymer that involves the complex inside of its structure, (➜) Removing the template molecules from the obtained polymer. A molecular recognition site for the target compound, in which functional monomer is

CONTACT Takuya Kubo ✉ kubo.takuya.6c@kyoto-u.ac.jp 🖳 Department of Material Chemistry, Graduate School of Engineering, Kyoto University, Katsura, Nishikyo-ku, 615-8510 Kyoto, Japan

three-dimensionally immobilized, has been prepared by above-mentioned procedures.

Generally, hydrogen bonding between the functional monomer and the template molecule is used to create the molecular recognition site. An externally stimulus-responsive MIP that can controllably release the target compound can be prepared because hydrogen bonding can be cleaved by the variations of temperature and/or pH conditions [8–12]. There is increasing expectation of the stimulus-responsive MIP for various fields other than analytical chemistry.

The most notable application of the stimulus-responsive MIP is the use as a carrier in a drug delivery system (DDS). The stimulus-responsive MIP is considered as a suitable material for a DDS carrier that can control a drug releasing rate depending on an external stimulus [13–15]. However, following cons are currently recognized, firstly unsatisfactory directivity toward the target area, in other words, self-directed delivery to diseased site is difficult due to a simple composition of the MIP using only organic polymer. Secondly, difficulty of a precise control of the drug releasing rate due to its large dependence on the environmental conditions such as temperature and/or pH. For solving these issues, we conceived an application of organic–inorganic hybrid material consisting of an MIP and magnetic thermal seed (MTS, Fe_3O_4) [16–19]. An MTS sized less than 20 nm exhibits superparamagnetic property and possesses considerable saturation magnetization giving the directivity toward the target area [20,21]. Additionally, it is known that the MTS generates heat under an alternate current (AC) magnetic field because of the relaxation of the magnetic moment, and the amount of generated heat can be controlled by modulating the strength of the magnetic field [22–25].

Some studies on the DDS using an MTS have been reported. Corato et al. introduced MTS into the core of liposome then added a material that generated active oxygen by the laser irradiation. They successfully applied it to the thermotherapy under an AC magnetic field and the phototherapy under the laser irradiation [26–30]. However, the annihilation of cancer cells only by hyperthermia effect is considered difficult, and the concurrent use of anti-cancer drug treatment has been proposed. We are developing a novel drug carrier that affords controllable anti-cancer drug releasing and directivity toward the diseased site by an MTS coated with a thermal-responsive MIP. The concept of this system will be advantageous compared to other techniques because an MTS contributes induction and heat generation, and an MIP contributes thermo-responsive drug release.

In our previous study, the selective adsorption and desorption of methotrexate (MTX), a commonly used anti-cancer drug, which prohibits the metabolism of folic acid (antifolic drug), was succeeded by using a thermal-responsive MIP, in which the hydrogen bonding based molecular recognition site was created with methacrylic acid (MAA) as a functional monomer [31]. However, the small releasing rate for MTX and the significant agglomeration were remaining problems to be improved for the use as a DDS carrier in both the MTS and MIP parts. In the former, the aggregation of the particles and the lack of generated heat amount [32] should be considered, whereas the limited biocompatibility and the lack of adsorption selectivity due to the structural hydrophobicity of an MIP in the latter. Additionally, particle size being larger than 1 μm for the hybridized material after the vinyl group introduction should also be improved.

Due to these drawbacks, here we try to address the following issues in this study. Firstly, MTS-related issues; novel uniformly sized MTS was prepared by using the oleic acid (OA)-added thermal decomposition method that provided the suppressed aggregation and controlled seed size [33–35] to increase the heat generation [20,23,25]. Secondly, MIP related issues; new MIP targeted to pemetrexed (PMX), anti-cancer drug, which is also an antifolic drug as well as MTX, was prepared with diethylaminoethyl methacrylate (DEAEMA) as a functional monomer and ethylene glycol dimethacrylate (EDMA) as a crosslinker to improve the biocompatibility. PMX exhibits larger solubility against typical organic solvents, resulting in high density of the molecular recognition site compared with MTX. Additionally, PMX is expected to afford stronger anti-cancer effect as well. Thirdly, the hybridization of the MIP and MTS; previously reported vinyl group introduction was changed from 'via silica coating' to 'via ligand exchange' to prepare smaller than 200 nm [36–38] size of the particle that is suitable as the functionalized DDS carrier [39–41] considering the internal-body circulation and the enhanced permeation and retention effect on the cancer tissue. One on one MIP coating on the MTS is preferable.

2. Materials and methods

2.1. Chemicals

2-Propanol (extra pure reagent), toluene (extra pure reagent), methanol (HPLC grade), formic acid, *N,N*-dimethylformamide (DMF) (extra pure reagent), ethanol (HPLC grade), dimethyl sulfoxide (DMSO) (extra pure reagent), tetrahydrofuran (THF) (extra pure reagent), acetonitrile (HPLC grade), benzoic

acid, distilled water (HPLC grade), acrylic acid, monomer (AA), hexane (HPLC grade) and divinylbenzene (DVB) were purchased from Nacalai Tesque, Inc. (Kyoto, Japan). OA, uracil, MAA and 2,2′-azobis(2,4-dimethylvaleronitrile) (ADVN) were purchased from Wako Pure Chemical Industries, Ltd. (Tokyo, Japan). PMX, 2, 2′-azobis(isobutyronitrile) (AIBN), N-carbobenzoxy-L-glutamic acid (NCLG), 2-(diethylamino)ethyl methacrylate (stabilized with MEHQ) (DEAEMA), N-[(9H-fluoren-9-ylmethoxy)carbonyl]-L-aspartic acid (L-FAA), N-[(9H-fluoren-9-ylmethoxy)carbonyl]-D-aspartic acid (D-FAA) and EDMA (stabilized with HQ) were purchased from Tokyo Chemical Industry Co., Ltd. (Tokyo, Japan). DEAEMA, EDMA and DVB were used after distillation. 1-Octadecene and goethite were purchased from Sigma-Aldrich (Tokyo, Japan). 14G-DMA was kindly donated from Shin-Nakamura.

2.2. Instrumentation

An HPLC system consisted of a pump (LC-30AD), a degasser (DGU-20A₅R), a column oven (CTO-20AC) and a photodiode array detector (SPD-M20A) (Shimadzu Co., Kyoto, Japan). A Thermomixer C (Eppendorf AG. Hamburg, Germany) was used as a shaker. A direct mixer DM-301 (AS ONE Co. Tokyo, Japan) was used as a mechanical stirrer, and a TM-VSM 1230-HHH5 (Tamakawa Co., LTD, Sendai, Japan) was used as a vibrating sample magnetometer. A Nicolet iS5 ATR (Thermo Fisher Scientific Inc. Waltham, MA, USA) was used as an FT-IR spectrometer. A T162-5723A (Thamway Co. Ltd., Shizuoka, Japan) was used as an AC magnetic field generator, and an H-103NR (Kokusan Co. Ltd. Saitama, Japan) was used as a centrifuge. A Zetasizer Nano ZSP (Malvern Panalytical, Malvern, UK) was used for dynamic light scattering (DLS) measurements. A 2510J-MT (Branson Co. Ltd, Atsugi, Japan) was used as a bench-top ultrasonic cleaner. An H-8100 (Hitachi Ltd, Tokyo, Japan) was used as a transmission electron microscope. HPLC conditions were as follows; mobile phase, 0.1% (v/v) formic acid aq./methanol = 65:35; flow rate, 2.1 mL/min; column, Mightysil RP-18GP II (150 mm × 2.0 mm, particle size 3 μm); detection, UV at 254 nm.

2.2.1. Preparation of MTS
The MTS was prepared by the following procedures. A mixture of 1-octadecene (10.0 g), OA (10.0 g) and goethite (0.534 g), which is the most common of the iron oxyhydroxides and is anti-ferromagnetic with a disordering (Néel) temperature was sonicated in a four-necked flask. After a 6 h stirring under the

conditions of programmed N_2 supply (50, 100, 125 and 150 mL/min) and thermal treatment at maximum 315 °C, the obtained each MTS was collected by a magnetic decantation method, then washed with a mixture of toluene/2-propanol = 1:6 (v:v). Each MTS was dried and subjected to the evaluation for dispersity using TEM and DLS.

2.2.2. Evaluation of MTS using XRD and VSM
The crystal structure of the obtained MTS was determined with XRD and the magnetic characteristics was evaluated with VSM.

2.2.3. Measurement of head generation of MTS under AC magnetic field
The dried MTS was dispersed in toluene (20.7 mg/ 2 mL), then treated with ultrasonication. The dispersed solution was set in the center of the coil to be applied with the AC magnetic field of 600 kHz and 3.2 kA/m. The specific adsorption rate (SAR) was calculated based on the temperature variation measured with the optical fiber thermometer using the following formula

$$SAR = C_S(m_S/m_i) \ (dT/dt)_{initial}$$

where C_S is specific heat of the solvent, m_S is amount of the solvent, m_i is amount of magnetic particles and (dT/dt) is differentiation of temperature per unit time, respectively.

2.3. Preparation and evaluation of MIP

Four MIPs and their related NIPs listed in Table S1 and Figure 1 were prepared and evaluated under appropriate conditions. Here, we chose two basic functional monomers, 4VP and DEAEMA at four times mole ratio toward template molecules. We anticipated that these monomers effectively interacted with the carboxy groups in both PMX and NCLG. After brief adsorption test of the four MIPs using target PMX or template NCLG, further detailed evaluations were executed on the most promising MIP4. Adsorption test in 1 mL of NCLG acetonitrile solutions at 1.0, 2.5, 5.0, 7.5, 10, 15, 20, 25, 30, 50, 100, 250, 500, 750, 1000 μM containing 5.0 mg of MIP4 and NIP4, respectively was carried out for 24 h stirring at 800 rpm. The filtered supernatants were determined with HPLC to calculating the binding constants using following formula

$$Q/C = nK - KQ$$

where Q is amount of bounded MTX (mol g^{-1}), C is concentration of free MTX (M), n is number of the binding sites (mol g^{-1}) and K is binding constant (M^{-1}). Adsorption test in 1.0 mL of PMX under the same conditions as the above but at the concentrations of 500 and 1000 μM was carried out.
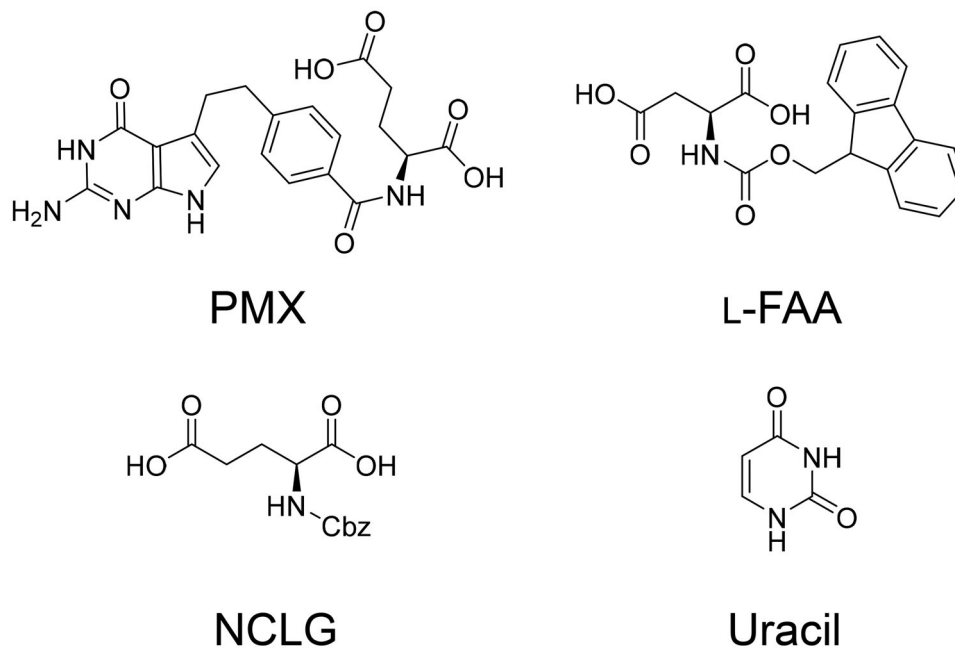
Figure 1. Structural analogues of PMX and NCLG employed for the evaluation.

Adsorption selectivity test for following structural analogues of PMX under similar conditions as the above but only at a concentration of $1000\,\mu$M was carried out. Desorption test of PMX from the MIPs tested in (2.4) evaluation. Two MIPs of the dried 2.0 g were added into methanol of 1 mL at $25/60\,°$C for $10/60$ min, then the filtered supernatants were determined with HPLC. The imprinting factor (*IF*) was calculated by the following equation

$$IF = \text{(adsorption amount on MIP)} / \text{(adsorption amount on NIP)}$$

2.4. Ligand exchanging for MTS

The prepared OA coated MTS was subjected to the ligand exchange procedures to introduce vinyl groups as MAA preparing for flat MIP coating under mono-dispersity conditions.

1. 3.6 mL of MAA and 0.4 mL of water were treated with ultrasonication for 10 min.
2. 4 mL of OA-MTS hexane solution (25 mg /mL) was treated with ultrasonication for 10 min.
3. MAA ligand solution was transferred into a sample vial then OA-MTS hexane solution was added to make 13.5 mL.
4. Yielded MTS was recovered using a magnetic decantation after standing for 6 h then washed with ethanol.
5. MTS was re-dispersed into ethanol, DMSO and acetonitrile then subjected to TEM observation and DLS measurement.
6. MTS dispersed into ethanol was recovered using a magnetic decantation method then subjected

to an infrared spectroscopy (IR) measurement following an overnight vacuum drying.

2.5. Example polymer coating on MTS after ligand exchange

The hybridization of the MTS and three types of polymers as the model of MIP was preliminary tried following the previous studies [32,41]. The MAA-MTS obtained from ligand exchange was hybridized with blank polymers, which have no imprinted site, listed in Table S2. Other conditions are also shown in Table S2. The yielded MTS based particles were recovered using magnetic decantation then washed with methanol and re-dispersed in DMSO to be subjected to the TEM observation and DLS measurement.

3. Results and discussion

3.1. Preparation of MTS

Figure 2 summarizes the physical appearances of the prepared MTS. Figure 2(a) shows the TEM image of the prepared MTS. The mean diameter and its relative standard deviation (RSD) were estimated as 14.1 nm and 4.7% ($n = 200$), respectively, based on the image. Less than 5% of the particle size RSD suggested the successful mono-dispersed preparation of MTS. The MTS kept a well-dispersed state for a while in toluene (Figure 2(b)). Magnetic decantation of the MTS was successfully executed in toluene/2-propanol $= 1$:6 (Figure 2(c)) suggesting that the directional control of MTS could be possible by the AC magnetic field. Figure 2(d) shows the result of the DLS measurement and the calculated mean diameter was 18.7 nm. The value was slightly larger
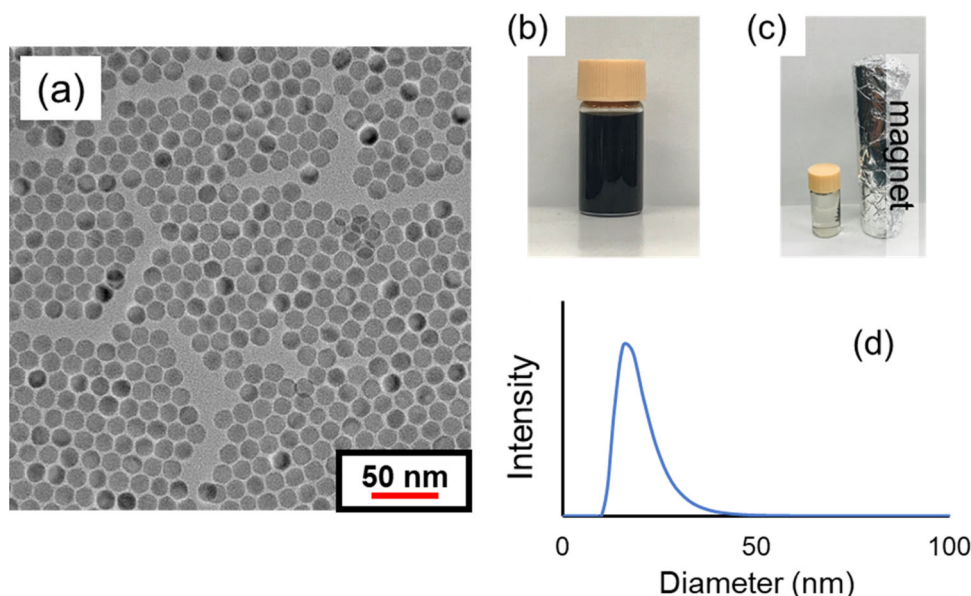
京都大学
KYOTO UNIVERSITY

京都大学学術情報リポジトリ
KURENAI 紅
Kyoto University Research Information Repository

NANOCOMPOSITES 219

Figure 2. Physical appearance of the MTS. (a) TEM image, (b) dispersion, (c) magnetic decantation, (d) result of DLS.
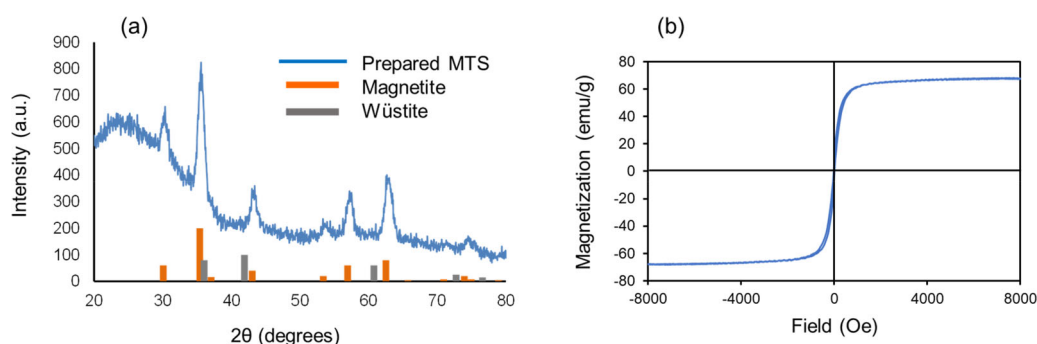

Figure 3. X-ray diffraction profile of MTS and standard spectra from magnetite and Wüstite (a), magnetization curve of MTS (b).
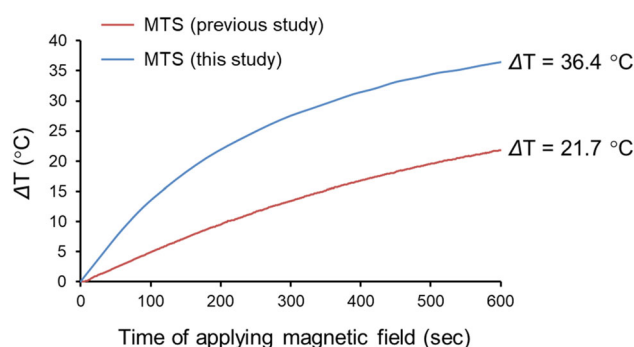
Figure 4. Temperature variation versus applied time of AC magnetic field.

compared to the result from TEM, and it assumed that the MTS after drying and re-dispersion into the solvent generated some amount of aggregations.

3.2. Heat generation of MTS under AC magnetic field

Figure 3(a) shows the X-ray diffraction profile of the MTS that was assigned to Fe_3O_4 (ICDD powder diffraction data No. 00-019-0629) based on the peak position and peak intensity ratio. It was revealed that Wüstite, which is a mineral form of iron(II) oxide found in meteorites and native iron, phase, having no heat-generating ability, was not contained in the MTS according to no significantly assigned peak to that from the Wüstite spectrum. Furthermore, Figure 3(b) shows the magnetization curve of the MTS at room temperature (maximum externally applied magnetic field; 8 kOe). The saturated magnetization was 67.99 emu/g, which was similar to measured value in our previous studies [23]. The possibility of external directional controlling for MTS was suggested because
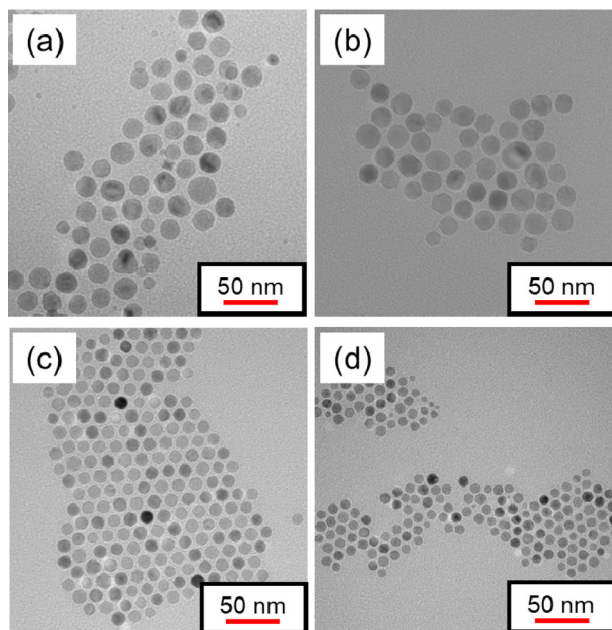
Figure 5. TEM images of MTS obtained under different N_2 supplying conditions.

Table 1. RSD values of TEMs based on TEM images in different N_2 supplying conditions ($n = 200$).

N_2 (mL/min)	(a) 50	(b) 100	(c) 125	(d) 150
TEM diameter (nm)	17.2	18.2	11.9	11.3
RSD (%)	18	9.0	7.5	8.0

of its super paramagnetic property approved by the absence of a hysteresis loop.

3.3. Measurement of heat generation of MTS under AC magnetic field

Time dependent temperature variation of the MTS under the AC magnetic field, frequency $f = 600$ kHz and strength $H = 3.2$ kA/m are shown in Figure 4. The result from previous study that employed the coprecipitation method is also shown for the reference. Present MTS prepared by the thermal decomposition method provided an improved heat-generating ability in the first 10 min. Considering the different dispersion solvent to that of the previous study, the SAR values for respective MTSs were calculated for the fair comparison. The present MTS showed 8.9 W/g which was larger than 7.3 W/g from data reported from previous MTS [32]. Consequently, the improved heat-generating ability was confirmed.

3.4. Particle size control during MTS synthetic process

Figure 5 shows TEM images of the MTS in different N_2 supplying conditions (a, 50; b, 100; c, 125; d, 150 mL/min). Table 1 shows calculated particle diameters and their uniformity in RSD ($n = 200$). At

the 125 mL/min N_2 supplying, the highest uniformity and almost desired particle size of the MTS was successfully prepared. The large N_2 supplying provided small particle size. This would be due to the increased core formation rate induced by the increased reduction rate under N_2 atmosphere. Based on this result, it was suggested that the particle size was surely controlled by N_2 supplying amount. As shown in the previous study, the size and its degree of dispersion are very important for the heat generation under the AC field [20], therefore, the optimization process will also be contributed to the control of the degree of the heat generation.

3.5. Evaluation of MIPs

For the MIP-1, Figure S1 shows the results of the adsorption test for PMX. In the DMSO solvent, no significant adsorption was observed in the MIP-1 and NIP-1. This is due to the larger interaction between PMX and DMSO than that between PMX and the functional monomer. DMSO is not suitable solvent for preparing an MIP in which PMX is employed as the template.

For the MIP-2, DMSO was not a suitable solvent for preparing MIP-2, whereas PMX was able to be dissolved into only DMSO to meet necessary concentration to create a molecular recognition site. Next NCLG was used as a pseudo template. NCLG is cheap and expected to interact with 4VP, the employed functional monomer. Figure S2 shows the results of the adsorption test for PMX. In methanol and acetonitrile, specific molecular recognitions were observed but the adsorbed PMX amount of 5 μmol/g was too small to be compared with density of the molecular recognition site of 50 μmol/g. The adsorption capacity of the MIP-2 was just 10% of expected value.

For the MIP-3, the adsorption test of the MIP-3 prepared with NCLG as a pseudo template and EDMA as a crosslinker is shown in Figure S3. Short chain length of EDMA provided improved adsorption but still not enough. Calculated adsorption efficiency was around 15% based on the number of recognition sites. This suggested that the creation of the molecular recognition site with 4-VP was not enough and/or the interaction with 4-VP was limited. For the MIP-4, this was prepared using DEAEMA as a functional monomer. The results of adsorption tests in 1000 μM of NCGL using various solvents are shown in Figure S4. Based on the results, a large adsorption capacity and high molecular recognition ability were confirmed. In the case of using higher concentration of NCLG, more than 90% of adsorption efficiency against the theoretical
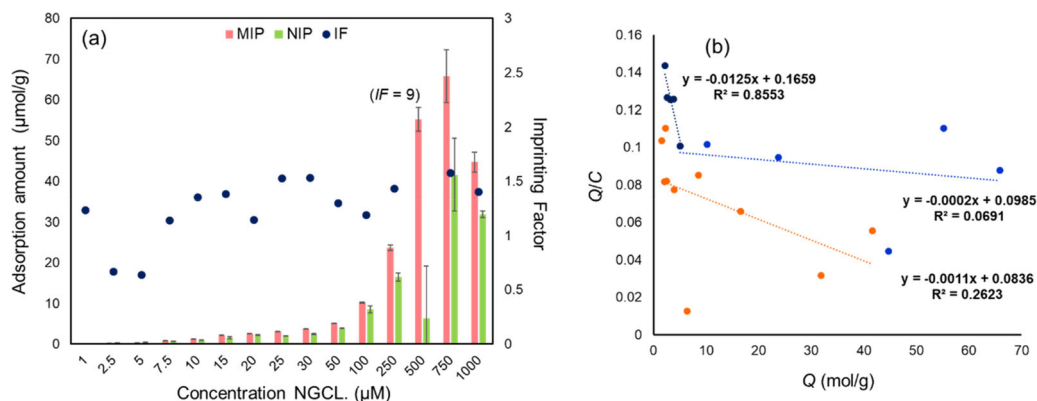
Figure 6. Adsorption capacities of MIP-4 and NIP-4 in various concentrations of NGCL (a). Scatchard plot for finally prepared MIP-4 and its NIP-4 for NCLG (b).

Table 2. Binding constant K calculated from Scatchard plot.

		K (M^{-1})
NIP-4		1.1×10^3
MIP-4	1–15 μM	1.2×10^4
	15–1000 μM	2.0×10^2

adsorption capacity (50 μmol/g) was observed in an acetonitrile and ethanol solution.

3.6. Adsorption test in different concentrations and estimation of binding constant (K)

The MIP-4 that consisted of EDMA as a crosslinker, DEAEMA as a functional monomer and NCLG as a pseudo template was subjected to further evaluations. Figure 6(a) shows adsorption capacities in various concentrations of NGCL. The molecular recognition abilities (IF is larger than 1) originating from imprinted sites were confirmed at 7.5 μM or higher. The adsorption efficiencies were almost 100% at the concentration of 500 μM or larger. Scatchard plot, in which the kinetics of ligand binding to receptors can be graphically represented in a variety of ways, was created based on the data of adsorption test in the range of more than 15 μM (Figure 6(b)). The tangent value of the plot is dramatically changed around the point of 5–6 μmol/g, which corresponds to 15 μM of the NCLG solution. When the mentioned point was considered as the inflection point, K for the NCLG concentration range of 1–15 and 15–1000 μM were 1.2×10^4 (M^{-1}) and 2.0×10^2 (M^{-1}), respectively. Largely changing because of the molecular recognition effect K was confirmed (Table 2).

3.7. Adsorption and desorption tests of the MIP toward the target compound PMX

Figure 7(a) shows the result of the adsorption test of the MIP toward the target compound PMX at two different conditions (500, 1000 μM, 1 mL). Selective adsorption capacity that was provided by

molecular recognition site created with the pseudo template was observed. Figure 7(b) shows the results of adsorption test of the MIP-4 toward various analogues of the target PMX. An adsorption selectivity to PMX was obviously shown.

Figure 7(c) shows desorption amount of PMX from the MIP-4 under different time and temperature conditions. Increased temperature of 60 °C afforded increased desorption amount of PMX, suggesting that the hydrogen bonding between PMX and NCLG, a functional monomer, was effectively cleaved at high temperature. The desorption amounts of PMX in 10 and 60 min were not so largely different, suggesting that the adsorption equilibrium was immediately accomplished and sensitive against the temperature variation. It is surely one of suitable features for DDS.

3.8. Ligand exchanging modification for MTS

Figure S5 shows the appearance of the solutions during the ligand exchanging process. As described in our previous report, MTS particles moved from upper hexane layer to lower water layer 6 h after starting decantation (Figure S5(a), (b)). After adding a hexane solution containing an MTS onto MAA aqueous solution, the MTS solubility was immediately reduced and transferring to the aqueous layer and precipitation was observed. In AA ligand exchange, there was no significant change during initial 10 min then after 1 h, the transfer to the aqueous layer was observed. After the removal of the solvent following 6 h decantation (Figure S5(c)), the MTS after AA ligand exchanging showed no magnetic decantation effect. After the vacuum drying, only an orange-colored oily substance was obtained. In some cases, the MTS was recovered but the recovering rate was too small. Consequently, all the ligand exchanging experiments were executed only with MAA.

The evaluation of a magnetic property and dispersity was carried out for the ligand exchanged
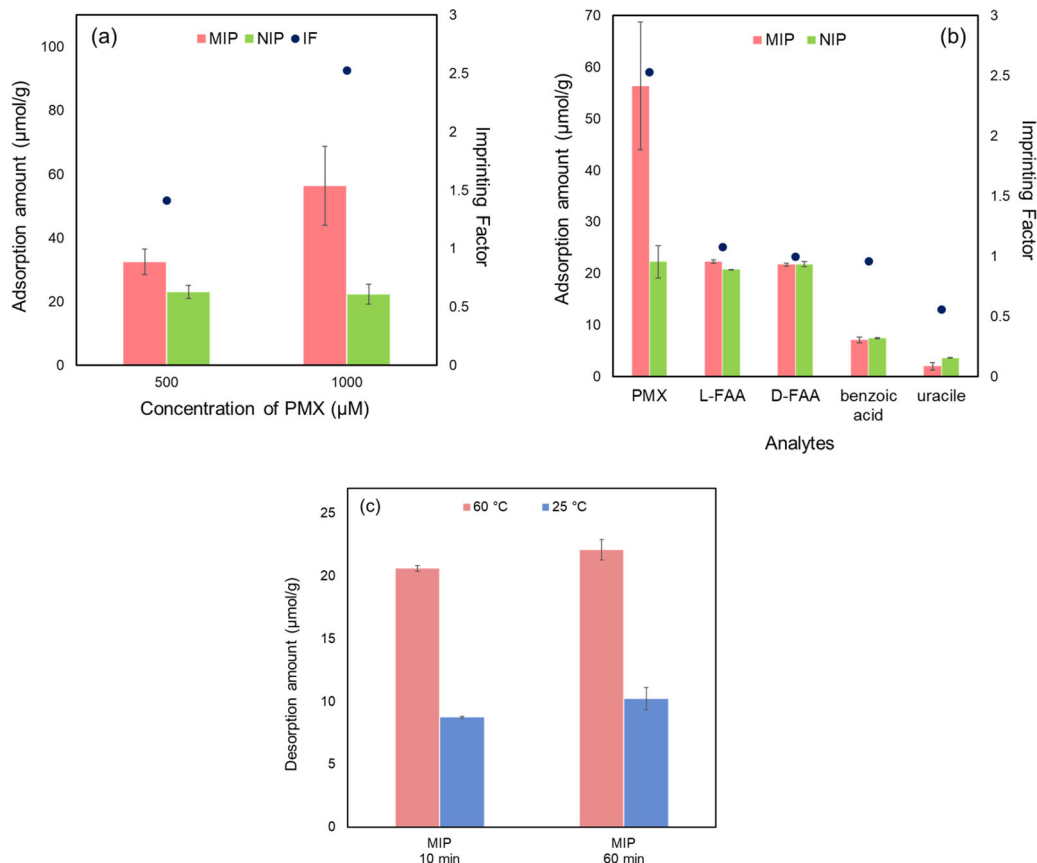
Figure 7. Adsorption and desorption test of MIP-4 toward PMX. Difference of the concentration of PMX (a), adsorption test of MIP4 toward various analogues of PMX (b) and desorption evaluation of MIP-4 for PMX at different time and temperature (c).
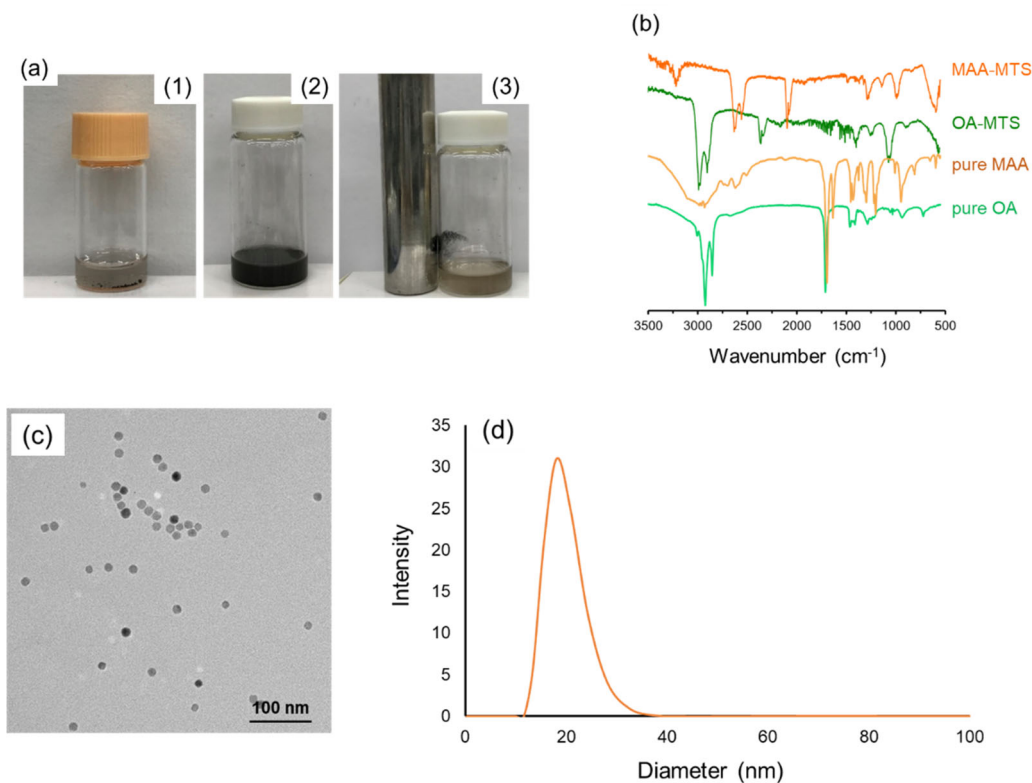
Figure 8. MTS behavior in (a) (1) OA-MTS in ethanol, (2) MAA-MTS in ethanol, (3) recovery with magnet of MAA-MTS, IR spectra (b), TEM (c) and DLS (d) of MAA-MTS.

MTS (MAA-MTS). The MAA-MTS was re-dispersed in ethanol and recovered using a strong magnet. The recovery behavior was the same as that of the

OA-MTS, before ligand exchange (Figure 8(a-1)). The OA-MTS was still precipitated in ethanol after 10 min ultrasonication. On the other hand, the

MAA-MTS was easily dispersed into ethanol (Figure 8(a-2, 3)), suggesting that the surface hydrophobicity of the MTS was increased after ligand changing from OA to MAA. Additionally, IR spectra of pure OA, pure MAA, OA-MTS and MAA-MTS are shown in Figure 8(b). Specific C–H stretching vibration at $2850–3000\,cm^{-1}$ from the OA-MTS was observed in the OA-MTS spectrum but disappeared in the MAA-MTS spectrum. The peaks at 1450, $1550\,cm^{-1}$ in the MAA-MTS spectrum were from symmetric and asymmetric vibration of coordinated carboxylic groups to Fe. Based on the results of IR analysis, it was suggested that ligand exchange was successfully executed. Finally, the physical properties of MAA-MTSs were evaluated using TEM and DLS. Figure 8(c) shows the TEM image and (d) shows the particle size distribution obtained by DLS. The particle size and the dispersion property were similar to those of OA-MTS. The DLS based mean particle size of the MAA-MTS was 19.6 nm, which was almost the same as the calculated particle size using the TEM image. This means no serious aggregation occurs in the MAA-MTS solution and mono dispersion maintained after the ligand exchange.

3.9. Polymer coating on MAA-MTS

Figure S6 shows the TEM images of the polymer coated MTS. The P-A1 coated with DVB provided partial coating but two or more MTS particles were included in the continuous polymer coating and mean size of the formed hybrid composition was larger than 500 nm. Some of MTS particles were not coated with DVB, and remained in dispersed state. The PA-2 with decreased DVB addition provided completely dispersed MTS without polymer coating (Figure S6(b)). On the other hand, the PB-2 with EDMA provided reasonably well-dispersed coated particles but in unexpected large particle size due to delocalized aggregation of EDMA monomers (Figure S6(c)).

The particle size distributions of respective polymer coated MTS are shown in Figure S7. The PA-1 showed the large size distribution in the TEM observation. The P-A2 showed a similar particle size distribution to that of the MTS after ligand exchanging. On the other hand, the P-B1 showed bimodal size distribution derived from small hybridized compositions including non-coated MTS and large aggregates. Based on these results, the hybridization, in other word, polymer coating of MTS was partially accomplished but the complete one-to-one hybridization of MTS was not succeeded. The ligand exchange method resulted in smaller aggregates than from silica coating. Consequently, after appropriate optimization of hybridization, an MIP coated MTS of smaller particle size can be prepared.

4. Conclusion

In this study, we prepared a novel hybrid carrier of a thermal-responsive MIP and an MTS that can control drug release by generating heat and directivity toward the diseased area and improved MTS, MIP and their hybridization based on our previous study. The method for precise formation of an MTS core using thermal decomposition was successfully established. Mono-dispersed and uniformly sized MTS preparation was confirmed by TEM observation and DLS measurement. This MTS particle having optimized particle size and its distribution showed obviously improved the heat-generating ability compared with an MTS particle prepared by coprecipitation method. Furthermore, we succeeded to control MTS particle size by changing N_2 supply during the thermal decomposition process. This means that MTS with optimized particle size for heat generation under various AC magnetic fields can be designed and prepared.

The MIP targeted for PMX, an anti-cancer drug, was prepared with the pseudo template NCGL, which afforded specific recognition to PMX and extremely increased number of recognition sites contributing to the improvement of the adsorption capacity. Basic functional monomer DEAEMA employed in place of 4VP resulted in an excellent selectivity to PMX and increased availability of the recognition site. This finally prepared MIP that consisted of EDMA as a crosslinker, DEAEMA as a functional monomer and NCLG as a pseudo template showed a specific molecular recognition to PMX among its various analogues and a satisfactory desorption characteristic for PMX derived from cleaving hydrogen bonding due to the generated heat by the MTS core. Based on these results, the possibility of a practical thermal-responsive DDS carrier was strongly suggested.

Disclosure statement

Funding

Notes on contributors

Takuya Kubo is an associate professor of Analytical Chemistry of Materials, Department of Material Chemistry, Graduate School of Engineering, Kyoto University. He received his Ph.D. from Kyoto Institute of Technology in 2004. After working as a Research Assistant in National Institute for Environmental Studies

(2001–2004), he joined Graduate School of Environmental Studies, Tohoku University as an assistant professor (2004–2012) and Department of Chemistry, Portland State University, OR, USA a visiting (2010–2011) (JSPS Excellent Young Researcher Overseas Visit Program), then moved to Kyoto University as an associate professor in 2012.

Miwa Shimonaka contributed to this work as a Ph.D. student. She received her master degree from Graduate School of Engineering, Kyoto University in 2021.

Yoshiyuki Watabe is a research fellow of Analytical Chemistry of Materials, Department of Material Chemistry, Graduate School of Engineering, Kyoto University. He worked in Shimadzu Corporation from 1984 to 2021 as an HPLC application engineer. During his employment period, he was sent to National Institute for Environmental Studies as a collaborative researcher in 2000. He received his Ph.D. from Kyoto Institute of Technology in 2005. Since 2021, he has worked in Kyoto University.

Kazunari Akiyoshi is a professor of Graduate School of Engineering, Kyoto University. He received his Ph.D. from Kyushu University in 1985. After working as an assistant/associate professor in Graduate School of Engineering, Kyoto University (1989–2002) and a professor in Tokyo Medical and Dental University (2002–2010), he moved to Kyoto University as a professor in 2010.

Jeyadevan Balachandran received his Ph.D. from Tohoku University in 1994. After working as an assistant professor and lecturer in Graduate School of Engineering, Tohoku University and Akita University, He became an associate professor in Tohoku University. Then he moved to The University of Shiga Prefecture as a professor in 2010.

Koji Otsuka received his Ph.D. from Kyoto University in 1986. After receiving the JSPS Fellowship for Young Scientists, he served as a senior lecturer/associate professor at Osaka Prefectural College of Technology (1988–1995) and an associate professor at Himeji Institute of Technology (1995–2002), followed by joining Kyoto University as a professor in 2002. His research interests include the development of micro/nano scale high performance separation techniques using electrophoretic and chromatographic methods, and their application studies mainly in bio-related and environmental analyses.

ORCID

Takuya Kubo (iD) http://orcid.org/0000-0002-9274-3295
Koji Otsuka (iD) http://orcid.org/0000-0003-1088-0569

References

1. Chen L, Wang X, Lu W, et al. Molecular imprinting: perspectives and applications. Chem Soc Rev. 2016;45(8):2137–2211.
2. Kubo T, Otsuka K. Recent progress for the selective pharmaceutical analyses using molecularly imprinted adsorbents and their related techniques: a review. J Pharm Biomed Anal. 2016;130:68–80.
3. Ansari S, Karimi M. Novel developments and trends of analytical methods for drug analysis in biological and environmental samples by molecularly imprinted polymers. TrAC, Trends Anal Chem. 2017;89:146–162.
4. Bazin I, Tria SA, Hayat A, et al. New biorecognition molecules in biosensors for the detection of toxins. Biosens Bioelectron. 2017;87:285–298.
5. Speltini A, Scalabrini A, Maraschi F, et al. Newest applications of molecularly imprinted polymers for extraction of contaminants from environmental and food matrices: a review. Anal Chim Acta. 2017;974:1–26.
6. Anantha-Iyengar G, Shanmugasundaram K, Nallal M, et al. Functionalized conjugated polymers for sensing and molecular imprinting applications. Prog Polym Sci. 2019;88:1–129.
7. Piletsky S, Canfarotta F, Poma A, et al. Molecularly imprinted polymers for cell recognition. Trends Biotechnol. 2020;38(4):368–387.
8. Pan J, Hang H, Dai X, et al. Switched recognition and release ability of temperature responsive molecularly imprinted polymers based on magnetic halloysite nanotubes. J Mater Chem. 2012;22(33):17167–17175.
9. Xu S, Lu H, Zheng X, et al. Stimuli-responsive molecularly imprinted polymers: versatile functional materials. J Mater Chem C. 2013;1(29):4406–4422.
10. Culver HR, Clegg JR, Peppas NA. Analyte-responsive hydrogels: intelligent materials for biosensing and drug delivery. Acc Chem Res. 2017;50(2):170–178.
11. Kim H, Jo A, Baek S, et al. Synergistically enhanced selective intracellular uptake of anticancer drug carrier comprising folic acid-conjugated hydrogels containing magnetite nanoparticles. Sci Rep. 2017;7(1):1–10.
12. Cazares-Cortes E, Cabana S, Boitard C, et al. Recent insights in magnetic hyperthermia: from the "hot-spot" effect for local delivery to combined magneto-photo-thermia using magneto-plasmonic hybrids. Adv Drug Deliver Rev. 2019;138:233–246.
13. Yin Q, Shen J, Zhang Z, et al. Reversal of multidrug resistance by stimuli-responsive drug delivery systems for therapy of tumor. Adv Drug Deliver Rev. 2013;65(13–14):1699–1715.
14. Karimi M, Ghasemi A, Zangabad PS, et al. Smart micro/nanoparticles in stimulus-responsive drug/gene delivery systems. Chem Soc Rev. 2016;45(5):1457–1501.
15. Zheng X-F, Lian Q, Yang H, et al. Surface molecularly imprinted polymer of chitosan grafted poly (methyl methacrylate) for 5-fluorouracil and controlled release. Sci Rep. 2016;6(1):1–12.
16. Ma H, Liu Y, Shi M, et al. Theranostic, pH-responsive, doxorubicin-loaded nanoparticles inducing active targeting and apoptosis for advanced gastric cancer. Biomacromolecules. 2015;16(12):4022–4031.
17. Zhu C, Yang G, Li H, et al. Electrochemical sensors and biosensors based on nanomaterials and nanostructures. Anal Chem. 2015;87(1):230–249.
18. Li J, Zhou Q, Yuan Y, et al. Iron-based magnetic molecular imprinted polymers and their application in removal and determination of di-n-pentyl phthalate in aqueous media. R Soc Open Sci. 2017;4(8):170672.
19. Zhang Z, Zhang X, Liu B, et al. Molecular imprinting on inorganic nanozymes for hundred-fold enzyme specificity. J Am Chem Soc. 2017;139(15):5412–5419.
20. De la Presa P, Luengo Y, Multigner M, et al. Study of heating efficiency as a function of concentration,

size, and applied field in γ-Fe2O3 nanoparticles. J Phys Chem C. 2012;116(48):25602–25610.

21. Kolosnjaj-Tabi J, Di Corato R, Lartigue L, et al. Heat-generating iron oxide nanocubes: subtle "destructurators" of the tumoral microenvironment. ACS Nano. 2014;8(5):4268–4283.

22. Park J, An K, Hwang Y, et al. Ultra-large-scale syntheses of monodisperse nanocrystals. Nat Mater. 2004;3(12):891–895.

23. Suto M, Hirota Y, Mamiya H, et al. Heat dissipation mechanism of magnetite nanoparticles in magnetic fluid hyperthermia. J Magn Magn Mater. 2009;321(10):1493–1496.

24. Kemp SJ, Ferguson RM, Khandhar AP, et al. Monodisperse magnetite nanoparticles with nearly ideal saturation magnetization. RSC Adv. 2016; 6(81):77452–77464.

25. Tong S, Quinto CA, Zhang L, et al. Size-dependent heating of magnetic iron oxide nanoparticles. ACS Nano. 2017;11(7):6808–6816.

26. Di Corato R, Béalle G, Kolosnjaj-Tabi J, et al. Combining magnetic hyperthermia and photo-dynamic therapy for tumor ablation with photoresponsive magnetic liposomes. ACS Nano. 2015;9(3): 2904–2916.

27. Deshpande S, Sharma S, Koul V, et al. Core–shell nanoparticles as an efficient, sustained, and triggered drug-delivery system. ACS Omega. 2017; 2(10):6455–6463.

28. Pei P, Yang F, Liu J, et al. Composite-dissolving microneedle patches for chemotherapy and photo-thermal therapy in superficial tumor treatment. Biomater Sci. 2018;6(6):1414–1423.

29. Yu L, Dong A, Guo R, et al. DOX/ICG coencapsulated liposome-coated thermosensitive nanogels for NIR-triggered simultaneous drug release and photothermal effect. ACS Biomater Sci Eng. 2018;4(7):2424–2434.

30. Albarqi HA, Wong LH, Schumann C, et al. Biocompatible nanoclusters with high heating efficiency for systemically delivered magnetic hyperthermia. ACS Nano. 2019;13(6):6383–6395.

31. Kubo T, Koterasawa K, Naito T, et al. Molecularly imprinted polymer with a pseudo-template for thermo-responsive adsorption/desorption based on hydrogen bonding. Micropor Mesopor Mat. 2015; 218:112–117.

32. Kubo T, Tachibana K, Naito T, et al. Magnetic field stimuli-sensitive drug release using a magnetic thermal seed coated with thermal-responsive molecularly imprinted polymer. ACS Biomater Sci Eng. 2019;5(2):759–767.

33. Roca A, Morales M, O'Grady K, et al. Structural and magnetic properties of uniform magnetite nanoparticles prepared by high temperature decomposition of organic precursors. Nanotechnology. 2006;17(11):2783–2788.

34. Niculaes D, Lak A, Anyfantis GC, et al. Asymmetric assembling of iron oxide nanocubes for improving magnetic hyperthermia performance. ACS Nano. 2017;11(12):12121–12133.

35. Mamiya H, Fukumoto H, Cuya Huaman JL, et al. Estimation of magnetic anisotropy of individual magnetite nanoparticles for magnetic hyperthermia. ACS Nano. 2020;14(7):8421–8432.

36. Mitra S, Gaur U, Ghosh P, et al. Tumour targeted delivery of encapsulated dextran–doxorubicin conjugate using chitosan nanoparticles as carrier. J Control Release. 2001;74(1–3):317–323.

37. Wong C, Stylianopoulos T, Cui J, et al. Multistage nanoparticle delivery system for deep penetration into tumor tissue. Proc Natl Acad Sci USA. 2011; 108(6):2426–2431.

38. Biswas S, Kumari P, Lakhani PM, et al. Recent advances in polymeric micelles for anti-cancer drug delivery. Eur J Pharm Sci. 2016;83:184–202.

39. Alvarez-Paino M, Marcelo G, Munoz-Bonilla A, et al. Surface modification of magnetite hybrid particles with carbohydrates and gold nanoparticles via "click" chemistry. Polym Chem. 2013;4(4):986–995.

40. Davis K, Cole B, Ghelardini M, et al. Quantitative measurement of ligand exchange with small-molecule ligands on iron oxide nanoparticles via radioanalytical techniques. Langmuir. 2016;32(51):13716–13727.

41. Kreissl P, Holm C, Weeber R. Frequency-dependent magnetic susceptibility of magnetic nanoparticles in a polymer solution: a simulation study. Soft Matter. 2021;17(1):174–183.